CCS Chemistry

RESEARCH ARTICLE

Received: Sept. 18, 2024 | Accepted: Dec. 3, 2024 | Published: Jan. 3, 2025

Modulating Static and Dynamic Magnetizations of Ytterbium(III) Coordination Polymers by Light-Induced Radicals

Xiaoshuang Gou[1], Yuewei Wu[1], Hanqi Wen[2], Liang Li[1], Wenlong Lan[1], Ning Liu[1], Shiqi Zhang[1], Liviu Ungur[2]*, Peng Cheng[1]* & Wei Shi[1]*

[1]*Frontiers Science Center for New Organic Matter, Key Laboratory of Advanced Energy Materials Chemistry (MOE) and State Key Laboratory of Advanced Chemical Power Sources, College of Chemistry, Nankai University, Tianjin 300071,* [2]*Department of Chemistry, National University of Singapore, Singapore 117543*

**Corresponding authors: chmlu@nus.edu.sg; pcheng@nankai.edu.cn; shiwei@nankai.edu.cn*

Cite this: *CCS Chem*. **2025**, Just Published. DOI: 10.31635/ccschem.024.202404999

Light-induced transformation from diamagnetic ligand to paramagnetic radical offers a unique approach to modulating the magnetization dynamics of magnetic compounds. In this study, we present a two-dimensional Yb(III) coordination polymer 1 and its Y(III)-diluted analog 1@Y, along with their light-induced radical forms, 1a and 1a@Y. Due to the presence of light-induced radicals, the magnetic susceptibility properties ($\chi_M T$ values) of 1a and 1a@Y featured remarkable 82.3% and 88.9% enhancements, respectively, at room temperature, compared with those of 1 and 1@Y, and were accompanied by an unexpected increase in the effective energy barrier for magnetization dynamics. The magnetization dynamics of 1 and 1a involved both Orbach and Raman processes, while 1@Y and 1a@Y exhibited two Raman processes, indicating that the Orbach process that occurred in 1 and 1a was mainly attributed to the magnetic coupling between Yb(III) ions. This work showcases the potential of light-induced radical transformation for tuning both the static and dynamic magnetic properties of lanthanide coordination polymers.

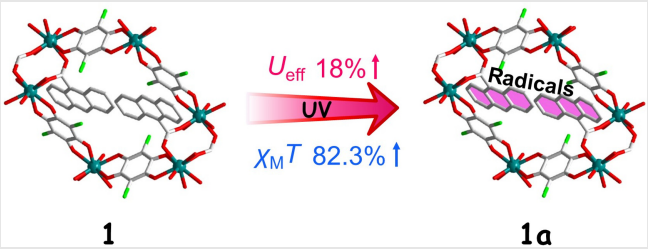

Keywords: **two-dimensional coordination polymers, ytterbium complexes, photomagnetism, single-molecule magnet, magnetization dynamics**

Introduction

Light-matter interaction is a promising way to modulate the physical properties of materials. Coordination compounds featuring light-induced radicals emerge as a platform for advanced photomagnetic materials across diverse applications.[1–6] Nevertheless, the impact of such radicals on magnetic properties is inherently complicated due to their instability and various interactions with other spin carriers.[7] Given the weak light-matter interactions, tuning magnetic properties via light irradiation within such materials is highly challenging.

Lanthanide coordination polymers present a special class of advanced magnetic materials based on their intrinsic large magnetic moments and strong magnetic anisotropy.[8,9] Optimizing the magnetization dynamics of

these polymers hinges on two critical factors: coordination symmetry and ligand field strength, both of which can be finely tuned through a coordination chemistry approach.[10,11] Alternatively, light irradiation is highly promising for modulating the magnetic properties of lanthanide coordination polymers. This not only enables the creation of photomagnetic materials but also provides valuable insights into magneto-structural correlations.[7,12–18] By incorporating ligands that transform to radical states after exposure to light, the pristine structures of lanthanide coordination polymers could remain unchanged. Consequently, these light-induced effects are confined to changes in the spin lattice rather than the atomic lattice of the materials. Hence, such systems are ideal for revealing the interplays between magnetism and spins, thereby facilitating the development of advanced photomagnetic systems.[18,19]

So far, for lanthanide coordination polymers, the study of magnetic properties has been mainly focusing on those containing Dy(III) ions because of their magnetic bistability.[13–19] However, other Kramers ions such as Er(III) and Yb(III) have received less attention.[7,20,21] Notably, the magnetization dynamics of Yb(III)-based compounds have been sparsely investigated due to their special coordination environments with f-electrons. Furthermore, most Yb(III)-based systems reported to date are discrete species.[22–28] The formation of extended structures with Yb(III) through metal-ligand coordination is beneficial for stabilizing the compounds, and hence, advantageous for the study of magnetization dynamics in the presence of light-induced radicals.

Herein, we report an Yb(III) coordination polymer [Yb(CA)(ACA)(DMF)(H_2O)]$_n$ (**1**, H_2CA = 2,5-dichloro-3,6-dihydroxy-p-quinone, HACA = 9-anthracene carboxylic acid), and its diamagnetic Y(III)-diluted analogue, **1@Y**. Irradiating **1** and **1@Y** by ultraviolet (UV) light generates **1a** and **1a@Y** (Scheme 1). The room-temperature $\chi_M T$ values of **1a** and **1a@Y** were significantly increased by 82.3% and 88.9%, respectively, in comparison to those of **1** and **1@Y**. It is worth noting that they are the highest increased $\chi_M T$ values influenced by light-induced radicals. Electron paramagnetic resonance (EPR) signals verified the light-induced radicals within **1a** and **1a@Y**, which also influenced the magnetization dynamics. **1** and **1a** featured Orbach and Raman processes, with the effective energy barrier, U_{eff}, of **1a** unexpectedly surpassing that of **1**. After dilution with diamagnetic ions, **1@Y** and **1a@Y** exhibited two Raman processes, rather than the Orbach and Raman processes observed in **1** and **1a**. This difference highlighted the impact of magnetic coupling on magnetization dynamic pathways within these Yb(III) coordination polymers. Ab initio calculations, based on density functional theory (DFT), revealed that the increase in magnetic susceptibility observed at high temperatures is attributed to the presence of unpaired electrons trapped in localized T_1 states of the ACA^- ligands.

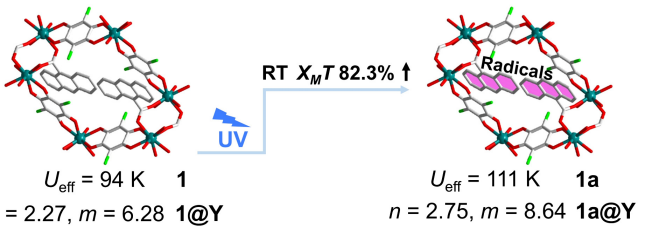

Scheme 1 | *The photochemical reaction from **1** and **1@Y** to **1a** and **1a@Y**. Color code: Yb/Y, cyan; O, red; Cl, green; and C, gray.*

Experimental Methods

Synthesis of [Yb(CA)(ACA)(DMF)(H_2O)]$_n$ (1)

$YbCl_3 \cdot 6H_2O$ (0.1 mmol, 38.7 mg), H_2CA (0.02 mmol, 4.2 mg), HACA (0.02 mmol, 4.5 mg), dimethylformamide (DMF) (2 mL), and H_2O (10 mL) were added into a 20 mL glass vial. The mixture was ultrasonicated for about 10 min to be completely dissolved. The glass vial was heated at 96 °C for 5 h. After cooling down to room temperature, brown hexagonal crystals were collected, washed with water (5 × 5 mL), and dried under air. Yield: 57.8% based on H_2CA. Anal. Calcd for $C_{24}H_{18}Cl_2NO_8Yb$: C, 41.63; H, 2.62; N, 2.02. Found: C, 41.48; H, 2.49; N, 1.79. Attenuated total reflection Fourier transform infrared (ATR-FTIR) spectroscopy, cm^{-1}: 3572 (w), 1666 (m), 1627 (w), 1582 (m), 1497 (s), 1456 (w), 1436 (w), 1376 (s), 1325 (w), 1296 (w), 1279 (w), 1112 (m), 1063 (w), 1005 (m), 884 (w), 871 (w), 849 (s), 791 (w), 774 (w), 733 (m), 684 (m), 674 (m), 651 (m), 604 (m), 579 (s), 562 (w), 463 (s), 449 (m), and 410 (m).

Synthesis of [$Yb_{0.12}Y_{0.88}$(CA)(ACA)(DMF)(H_2O)]$_n$ (1@Y)

1@Y was prepared by the same synthetic procedure as **1** with $YbCl_3 \cdot 6H_2O$ and $YCl_3 \cdot 6H_2O$ in a 1:7 molar ratio. Inductively coupled plasma-mass spectrometry (ICP-MS): Yb/Y = 1:7.50. Anal. Calcd for $C_{24}H_{18}Cl_2NO_8Yb_{0.12}Y_{0.88}$: C, 46.62; H, 2.93; N, 2.27. Found (**1@Y**): C, 46.84; H, 2.82; N, 2.18. FTIR (ATR, cm^{-1}): 3570(w), 1666 (m), 1627 (w), 1588 (m), 1497 (s), 1456 (w), 1436 (w), 1376 (s), 1327 (w), 1296 (w), 1279 (w), 1112 (m), 1061 (w), 1007 (m), 882 (w), 871 (w), 850 (s), 791 (w), 773 (w), 733 (m), 686 (m), 674 (m), 651 (m), 606 (m), 577 (s), 562 (w), 469 (s), 449 (m), and 410 (m).

Results and Discussion

1 and **1@Y** were prepared by reacting H_2CA and HACA with excess metal salts in DMF/H_2O solution. The resulting materials were characterized by elemental analysis, FTIR (Supporting Information Figure S1), powder X-ray

Citation: *CCS Chem.* **2025**, Just Published. DOI: 10.31635/ccschem.024.202404999
Link to VoR: https://doi.org/10.31635/ccschem.024.202404999

diffraction (PXRD) (Supporting Information Figure S2), thermogravimetry analysis (Supporting Information Figures S3 and S4), and solid-state UV–visible (UV–vis) absorption spectroscopy (Supporting Information Figures S5 and S6). Compound **1** crystallizes in the triclinic space group $P\bar{1}$ (Supporting Information Table S1). The crystallographically independent Yb(III) ion was eight-coordinated by four oxygen atoms from two CA^{2-}, two oxygen atoms from two ACA^{-}, one oxygen atom from H_2O, and one oxygen atom from DMF, exhibiting a distorted square antiprism geometry (D_{4d}, 1.191)[10] (Figure 1a, Supporting Information Figure S7 and Table S2). Two Yb(III) ions were bridged by oxygen atoms of two ACA^{-} to form a dimeric Yb_2 unit with a Yb···Yb distance of 4.608(7) Å (Figure 1b). Bond lengths of Yb-O_{CA} and Yb-O_{ACA} fall within the range of 2.308(3)–2.380(2) Å and 2.224(8)–2.337(8) Å, respectively, while Yb-O_{water} and Yb-O_{DMF} bonds are 2.392(3) and 2.284(3) Å, respectively. The O-Yb-O angles range from 66.44(10)–153.47(11)°. The dimeric Yb_2 units were linked by CA^{2-} to form one-dimensional chains along the *a*-axis (Figure 1c). These chains were connected by CA^{2-} to further construct a two-dimensional layer. The shortest Yb···Yb distance between neighboring layers was 9.576(3) Å (Supporting Information Figure S8a). A sandwich-like structure was formed by two ACA^{-} ligands close to one CA^{2-} ligand. The π···π stacking between $CA_{centroid}$ and $ACA_{centroid}$ is 3.672(8) Å (Figure 1d). Finally, these two-dimensional layers were stacked into a three-dimensional network (Supporting Information Figure S8b).

The time-dependent UV–vis spectra of **1** and **1@Y** were measured at room temperature (Supporting Information Figures S5 and S6). A broad absorption band appeared around 420 nm and increased under continuous UV light irradiation. The absorption intensity reached saturation after 30 min of irradiation, and remained unchanged for at least 1 h, indicating the stability of the light-induced radicals. Continuous-wave EPR measurements further confirmed these radicals, with single differential peaks at g = 2.0043 and 2.0037 for **1a** and **1a@Y**, respectively (Figure 2a,b, red lines). These g values were closely in line with those of HACA-based complexes,[7,29] characteristic of free radical species. Therefore, the radicals within **1a** were attributed to ACA^{-} and were stabilized by its conjugated structure. Without UV irradiation, **1** and **1@Y** also showed weak EPR signals (Figure 2a,b, black lines). These signals were tentatively ascribed to trace amounts of radicals within the samples generated by indoor light.[30,31] Additionally, the consistent FTIR and PXRD results measured before and after irradiation ruled out possible structural changes or photodecomposition of **1** and **1@Y** (Supporting Information Figures S1 and S2).

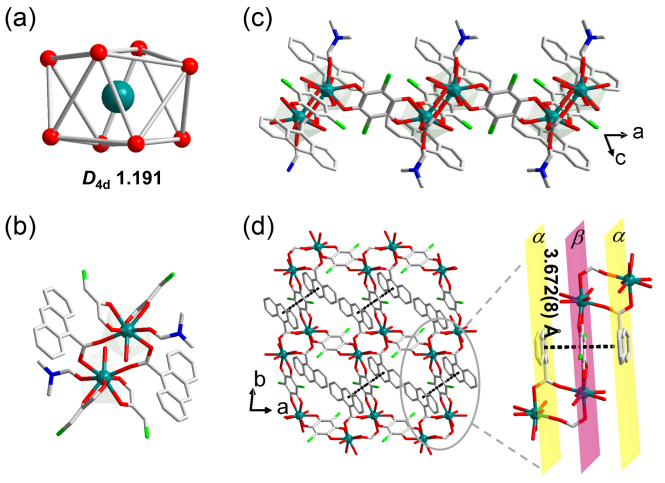

Figure 1 | *Coordination polyhedron of Yb(III) ion (a), dimeric unit (b), side view along* a*-axis (c), and a plane formed by π···π interactions between CA^{2-} and ACA^{-} (d) of **1**. Color code: Yb, cyan; O, red; N, blue; Cl, green; and C, gray.*

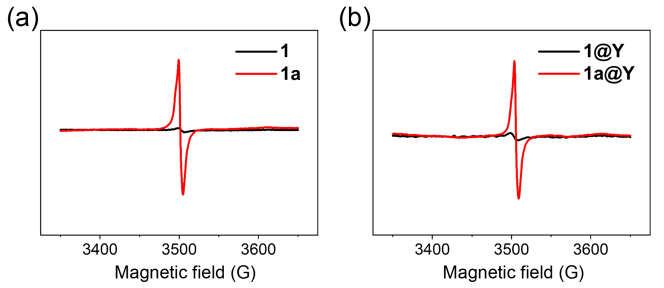

Figure 2 | *EPR spectra of **1** and **1a** (a), **1@Y**, and **1a@Y** (b).*

The magnetic properties of these compounds were measured using a superconducting quantum inference device (SQUID). Variable temperature magnetic susceptibilities of **1**, **1a**, **1@Y**, and **1a@Y** were collected under a 1000 Oe direct-current (dc) magnetic field. The room-temperature $\chi_M T$ value of **1** is 2.65 cm^3 K mol^{-1}, close to the theoretical value of 2.57 cm^3 K mol^{-1} for an isolated Yb(III) ion ($4f^{13}$, S = 1/2, L = 3, $^2F_{7/2}$, g_J = 8/7). The room-temperature $\chi_M T$ value of **1a** is 4.83 cm^3 K mol^{-1} (Figure 3a). Upon cooling, the $\chi_M T$ values of both **1** and **1a** decreased gradually to 1.45 cm^3 K mol^{-1} at 4 K and 1.45 cm^3 K mol^{-1} at 2.5 K, respectively, attributed to the depopulation of the M_J states.[32–35] For the diluted samples, **1@Y** and **1a@Y**, the room-temperature $\chi_M T$ values were 0.27 and 0.51 cm^3 K mol^{-1}, respectively (Figure 3b). Throughout cooling from 300 K to 2 K, the $\chi_M T$ values of **1@Y** and **1a@Y** decreased continuously due to the depopulation of the M_J states. The room-temperature $\chi_M T$ values for **1a** and **1a@Y** were 82.3% and 88.9% higher than those of **1** and **1@Y**, respectively, indicative of the formation of light-induced radicals, as reported in other literatures.[36,37] The increased $\chi_M T$ values were due to the large electron delocalization of the ligand within the entire two-dimensional framework that occurs after light

Citation: *CCS Chem.* **2025**, Just Published. DOI: 10.31635/ccschem.024.202404999
Link to VoR: https://doi.org/10.31635/ccschem.024.202404999

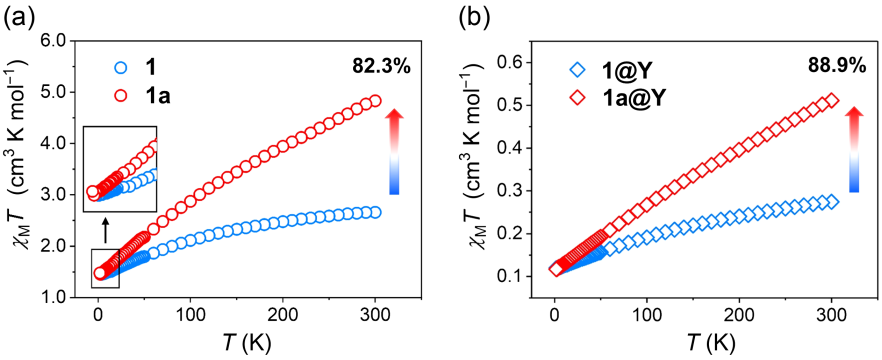

Figure 3 | *The χ_MT–T for **1** and **1a** (a), **1@Y**, and **1a@Y** (b).*

irradiation, discussed in detail under the "Ab initio calculation" section. It is worth noting that these increases of $\chi_M T$ values are the highest reported so far (Supporting Information Table S3).

The field-dependent magnetization was measured at 2, 3, and 5 K across an external magnetic field range of 0–70 kOe (Supporting Information Figure S9). The magnetization curves displayed a rapid ascent from 0 Oe to 15 kOe, reaching the values of 1.96, 2.09, 1.46, 1.50 $N\beta$ for **1**, **1a**, **1@Y**, and **1a@Y** at 70 kOe (T = 2 K), respectively. These values were all below the expected saturation value of 4 $N\beta$, as a result of strong magnetic anisotropy.[38–40] The hysteresis loops collected at 2 K reveal no discernible openings for the compounds (Supporting Information Figure S10). Furthermore, both the field-cooled and zero-field-cooled magnetic susceptibilities exhibited no divergences down to 2 K (Supporting Information Figures S11 and S12).

The alternating-current (ac) magnetization dynamics were investigated for **1**, **1a**, **1@Y**, and **1a@Y**. At zero dc field, the absence of magnetization dynamics was attributed to quantum tunneling of magnetization (QTM)[41,42] (Supporting Information Figure S13). However, when applying external dc fields of 200–3000 Oe at 2 K, a clear slow relaxation process was observed for **1** and **1@Y** (Supporting Information Figure S14), indicative of the suppression of QTM. The relaxation time (τ) maximizes at 800 and 600 Oe for **1** and **1@Y**, respectively (Supporting Information Figure S15). For **1**, **1a**, **1@Y**, and **1a@Y**, the in-phase (χ'_M) and out-of-phase (χ''_M) components of the ac susceptibility showed strong temperature and frequency dependence under the applied dc field (Figure 4a–d, Supporting Information Figures S16–S19).

Cole–Cole plots showed quasi-semicircles and were fitted by a generalized Debye model[43–45] (Figure 4e–h and Supporting Information Tables S4–S7). The determined dispersion coefficients (α) for **1**, **1a**, **1@Y**, and **1a@Y** were in the ranges of 0.022–0.266, 0.016–0.439, 0–0.170, and 0.023–0.224, respectively. To probe the relaxation mechanism, τ versus T were plotted logarithmically for **1**, **1a**, **1@Y**, and **1a@Y** (Figure 5a–d). The slopes of the locally weighted linear fits were 2.84, 4.36, 10.06 for **1**, 2.79, 4.67, 13.98 for **1a**, 2.88, and 5.43 for **1@Y**, 3.19 and 7.34 for **1a@Y**, indicative of multiple relaxation processes.[46,47] Magnetic relaxation processes include direct, Raman,

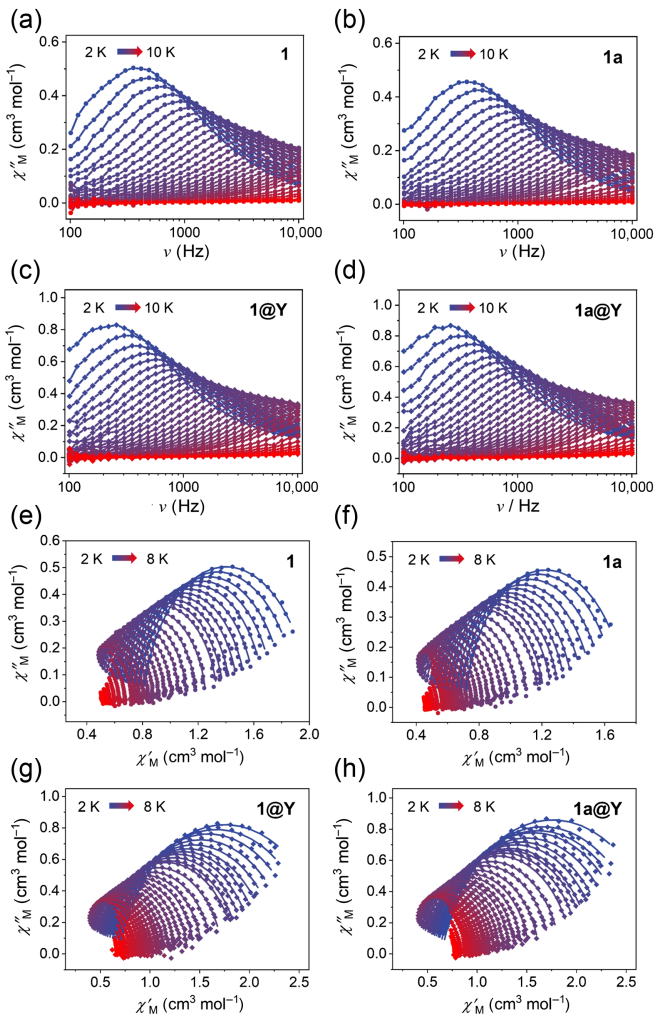

Figure 4 | *χ''_M vs ν for **1** (a) and **1a** (b), H_{dc} = 800 Oe, χ''_M vs ν for **1@Y** (c) and **1a@Y** (d), H_{dc} = 600 Oe; Cole–Cole plots of **1** (e) and **1a** (f), **1@Y** (g), and **1a@Y** (h).*

Citation: *CCS Chem.* **2025**, Just Published. DOI: 10.31635/ccschem.024.202404999
Link to VoR: https://doi.org/10.31635/ccschem.024.202404999

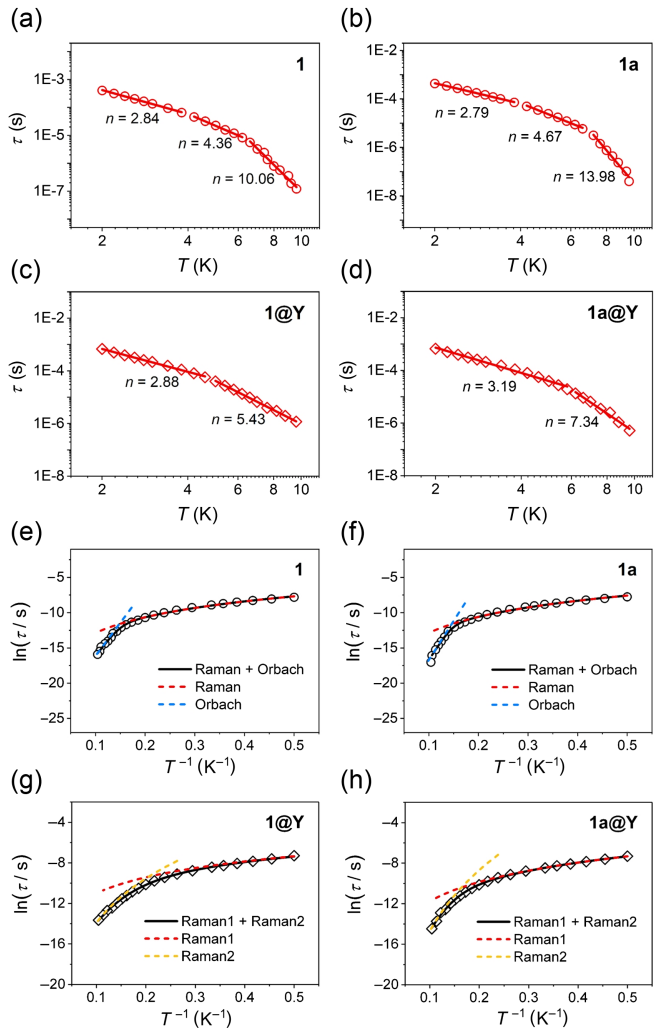

Figure 5 | *The plots of the relaxation time τ vs T on log–log scale for **1** (a), **1a** (b), **1@Y** (c), and **1a@Y** (d). Plots of ln(τ) vs T^{-1} for **1** (e), **1a** (f), **1@Y** (g), and **1a@Y** (h). The dotted red lines show $\tau^{-1} = AT^n$, the dotted yellow lines show $\tau^{-1} = CT^m$, the dotted blue lines show $\tau^{-1} = \tau_O^{-1}\exp(-U_{eff}/T)$, the solid lines show their sum, $\tau^{-1} = \tau_O^{-1}\exp(-U_{eff}/T) + AT^n$ for **1** and **1a**, $\tau^{-1} = AT^n + CT^m$ for **1@Y** and **1a@Y**.*

and Orbach processes, as well as quantum tunneling.[10,11] In the Raman process, the relaxation time decays with T^n, while the Orbach process featured an Arrhenius relationship between relaxation time and temperature, where U_{eff} was the energy barrier between the ground state and the excited state. Here, the relaxation times of **1** and **1a** were fitted by the expression $\tau^{-1} = \tau_O^{-1} \exp(-U_{eff}/T) + AT^n$, which comprised both Raman and Orbach processes. The fitting yielded U_{eff} = 94 K, τ_O = 8.25 × 10^{-12} s, A = 232.70 s^{-1} K^{-n}, n = 3.22 (R^2 = 0.9980) for **1**, U_{eff} = 111 K, τ_O = 8.77 × 10^{-13} s, A = 199.60 s^{-1} K^{-n}, and n = 3.29 (R^2 = 0.9986) for **1a**. In the literature, the U_{eff} values of magnetic coordination compounds usually decreased under light irradiation while examples with increased U_{eff} values were very limited (Supporting Information Table S8). The relaxation times of **1@Y** and **1a@Y** were fitted by the expression $\tau^{-1} = AT^n + CT^m$, which included two Raman processes, with A = 323.19 s^{-1} K^{-n}, n = 2.27, C = 0.56 s^{-1} K^{-m}, m = 6.28 (R^2 = 0.9994) for **1@Y**, and A = 225.20 s^{-1} K^{-n}, n = 2.75, C = 0.0054 s^{-1} K^{-m}, m = 8.64 (R^2 = 0.9992) for **1a@Y** (Figure 5e–h). The fitting results showed that the U_{eff} of **1a** was 18% higher than that of **1**. Additionally, the fitting parameters n and m for **1a@Y** were larger than those of **1@Y**. The temperature ranges of Raman and Orbach processes of **1** were 2–6.2 K and 6.2–9.6 K, which shifted to 2–7.0 K and 7.0–9.6 K for **1a**. The temperature ranges of the two Raman processes changed from 2–4.6 K and 4.6–9.6 K for **1@Y** to 2–5.8 K and 5.8–9.6 K for **1a@Y** (Table 1). These changes were attributed to light-induced radicals.

A summary of magnetization dynamics of Yb(III) coordination compounds is presented in Supporting Information Table S9. Notably, the magnetization dynamics of Yb(III) complexes influenced by light have not been reported to date. Since 2012, mononuclear and binuclear Yb(III) complexes have been studied, with binuclear Yb(III) complexes showing remarkable magnetization dynamics with Orbach, Raman, or direct processes.[23,48,49] The previously reported Yb(III) complexes possess Orbach process with U_{eff} values in the range of 7–77 K under applied dc fields, except for one example, [$^{173}Yb_{0.07}Y_{0.93}(tta)_3(L)]\cdot C_6H_{14}$ (tta^- = 2-thenoyltrifluoroacetonate and L = 4,5-bis(propylthio)tetrathiafulvalene-2-(2-pyridyl)benzimidazolemethyl-2-pyridine) with U_{eff} of 33 K under zero dc field.[50] In this study, we observed the highest U_{eff} of 111 K among Yb(III) complexes. The absence of Orbach processes for **1@Y** and **1a@Y** was ascribed to diamagnetic-ion dilution, which mitigated the interaction between Yb(III) ions. Our findings demonstrated the importance of magnetic interactions in enhancing magnetization dynamics.[35,51]

Ab initio calculations (OpenMolcas) for 1

Magnetic anisotropy of the Yb(III) site in **1** was established through ab initio calculations employing quantum chemistry programs used to calculate magnetic properties (CASSCF/RASSI/SINGLE_ANISO) type,[52] commonly employed for lanthanide compounds. The calculation

Table 1 | *Temperature Ranges of Magnetization Relaxation Processes for **1**, **1a**, **1@Y**, and **1a@Y***

Compounds	Temperature Ranges	
	Raman	Orbach
1	2–6.2 K	6.2–9.6 K
1a	2–7.0 K	7.0–9.6 K
	Raman1	Raman2
1@Y	2–4.6 K	4.6–9.6 K
1a@Y	2–5.8 K	5.8–9.6 K

Citation: *CCS Chem.* **2025**, Just Published. DOI: 10.31635/ccschem.024.202404999
Link to VoR: https://doi.org/10.31635/ccschem.024.202404999

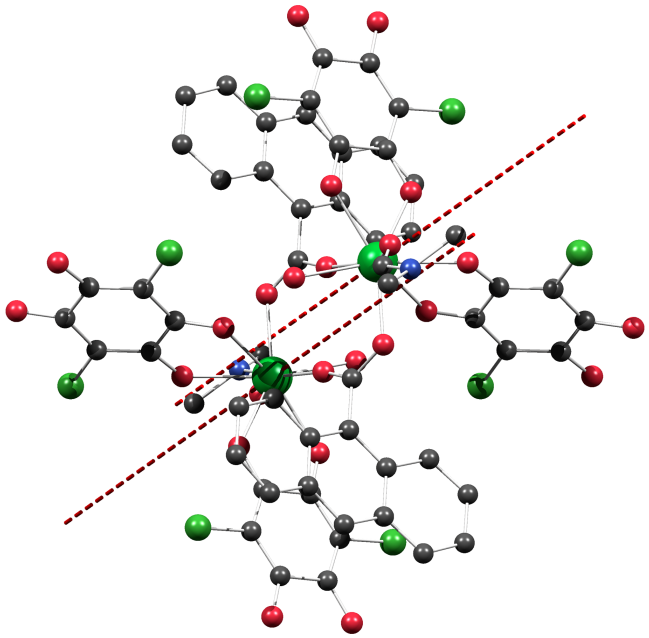

Figure 6 | *Orientation of the main magnetic axes on Yb (III) sites in **1**. Since the crystallographic structure does not change upon forming radicals and given the relatively localized nature of the organic radicals (vide infra), this orientation of local main axes remains the same in **1a**.*

results showed a strong splitting of ground multiplet $^2F_{7/2}$ by crystal field, bringing four Kramers doublets at 0.0, 193.2, 327.9, and 476.6 cm^{-1}. Subsequently, the excited $^2F_{5/2}$ multiplet was also subjected to crystal field splitting, yielding energy levels at 10348, 10527, and 10738 cm^{-1}. As a result of covalent and crystal field effects, the Yb(III) site in **1** exhibited one of the strongest uniaxial anisotropy observed by a Yb(III) compound, with g_X = 0.622, g_Y = 0.974, and g_Z = 7.36. All ab initio results are detailed in Supporting Information Tables S10 and S11, while Figure 6 illustrates the orientation of the local anisotropy axis with respect to the molecular frame. We notice that the local g_Z axes of Yb(III) sites featured a small angle with the plane of the carboxyl group of the ACA^- ligands, likely because of the shortest Yb–O bond formed by this carboxyl group. The magnetic exchange between Yb(III) sites in **1** was computed by the Broken-symmetry DFT method with optimized reaction coordinates algorithm (ORCA) software.[53,54] The results revealed very small antiferromagnetic values of magnetic interaction (Supporting Information Table S12), characteristic of exchange-coupled lanthanide compounds.

Solid state calculations of 1 and 1a with VASP

The formation of radicals in the system adds another dimension to the electronic structure problem. First, the radicals occupy diffuse orbitals (bands), exhibiting greater delocalization. Therefore, cluster fragmentation might induce significant perturbations to the electronic structure. To tackle this challenge, we performed periodic electronic structure calculations. Using the Vienna Ab Initio Software package (VASP), we conducted calculations to establish the band structure and density of states for the **1a** compound (Figure 7). Figure 8 shows the spin density (radicals) delocalization within the ligand framework, where the large electron delocalization in the ligand for **1a** is demonstrated.

Our proposed mechanism is presented as follows. Initially, radiation with 365 nm UV light triggers electronic transitions of up to 3.4 eV (~27,400 cm^{-1}). With this energy, both ligands of CA^{2-} and ACA^- in **1** could be excited to various excited states, typically to an excited singlet state (S_1, S_2, …, S_K, etc.) (Supporting Information Table S12). The lifetime of the excited state is usually short, with various optical and vibrational relaxation

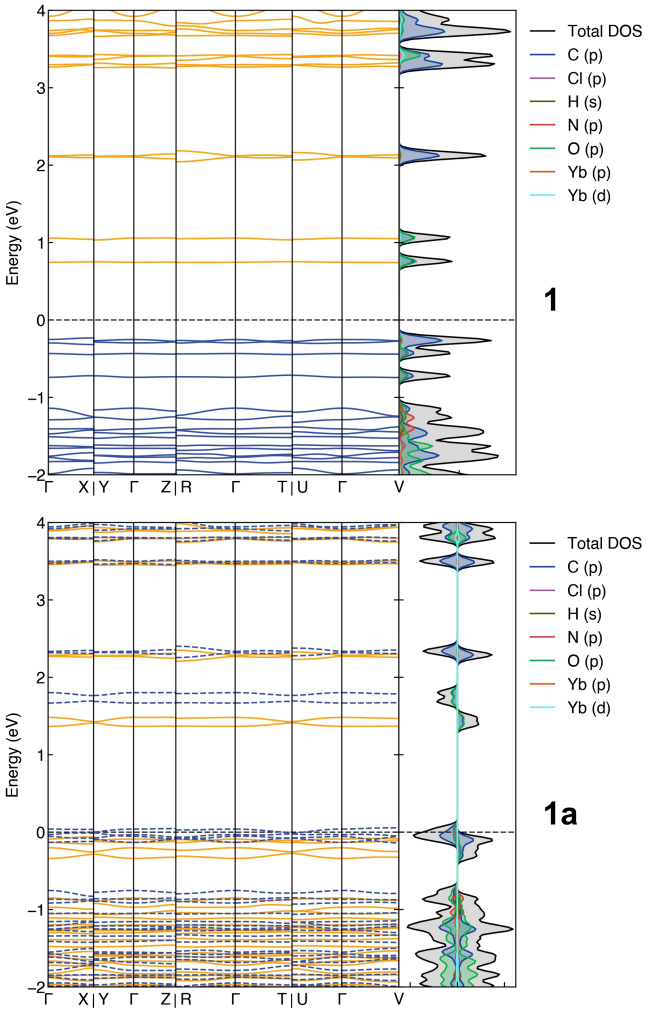

Figure 7 | *Band structure and density of states for **1** and **1a** compounds. The calculation for the **1a** system included two unpaired electrons (with spin-up) in each unit cell (NUPDOWN = 2). The Yb 4f electrons were treated in VASP calculations as part of the metal's core.*

Citation: *CCS Chem.* **2025**, Just Published. DOI: 10.31635/ccschem.024.202404999
Link to VoR: https://doi.org/10.31635/ccschem.024.202404999

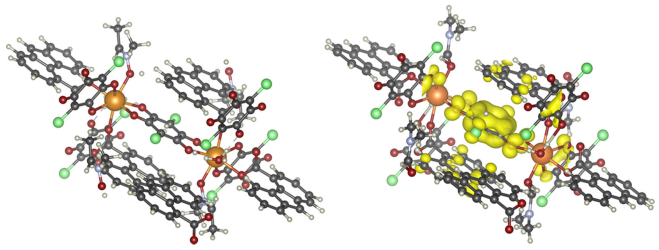

Figure 8 | *The spin-density plots of **1** (left) and **1a** (right).*

processes (both radiative and nonradiative) leading to energy loss and returning the system to its S_0 ground state. Following an intersystem crossing (ISC) process, the energy of the excited singlet state might transition toward certain triplet states (T_1, T_2, T_3, etc.). Various dynamical processes of excitations facilitate energy transfer within **1a**. While optical relaxation from the excited triplet states towards the S_0 ground state is generally forbidden, the spin–orbit coupling effect (phosphorescence) opens a relaxation pathway via singlet-triplet mixing. In the present case, the phosphorescence was significantly suppressed, particularly in the case of ACA^- ligands. From the calculations of individual ligands, the phosphorescence rate (i.e., the rate of $T_1 \rightarrow S_0$ transition) in the ACA^- ligand is ~307 times smaller compared to the CA^{2-} ligand (Supporting Information Table S13). In the case of the extended system such as **1a**, the excited triplet states interacted with each other and with other nearby spin states, diminishing the probability of transition towards the S_0 ground state. This led to an entrapment of excitations in the T_1 state localized at the ACA^- ligands. The steady increase in magnetic susceptibility observed at high temperatures was elucidated by the presence of numerous unpaired electrons trapped in localized T_1 states of the ACA^- ligands, which contributed to the total density of electronic states in the **1a** system.

Conclusion

In summary, we reported an Yb(III) coordination polymer and its Y(III)-diluted analog, both showing light-modulated magnetic properties. Upon irradiation of UV light, **1** and **1@Y** converted to radical-containing **1a** and **1a@Y**. The record increase of $\chi_M T$ values was due to the light-induced radicals at room temperature, which had the potential as a light-controlled molecular switch. Notably, **1a** displayed an unexpected enhancement of U_{eff} compared with **1**. The dilution experiment highlighted the significance of magnetic interactions between lanthanide ions in tuning magnetization dynamics, even in the presence of light-induced radicals. This work not only developed a strategy for achieving photomagnetic materials but also revealed the impact of light-induced radicals on the static and dynamic magnetization of lanthanide coordination polymers.

Supporting Information

Supporting Information is available and includes additional experimental details as well as supplementary figures (Figures S1–S19) and tables (Tables S1–S13).

Conflict of Interest

There is no conflict of interest to report.

Funding Information

This work was supported by the National Natural Science Foundation of China (grant nos. 20435002, 92156002, 21971123, and 62401563). L.U. acknowledges the financial support of the research projects A-800079-00-00, A-8000017-00-00, and A-8001894-00-00 of the National University of Singapore (NUS). Ab initio calculations were done on the Advanced Supercomputer for Petascale Innovation, Research and Enterprise 2A (ASPIRE-2A) cluster of the Singapore National Supercomputing Centre (NSCC; www.nscc.sg) under project 11001278. The high-performance computational (HPC) resources of NUS (HPC-NUS) are gratefully acknowledged. The NUS Research Scholarship program supported W.H.

References

1. Erbas-Cakmak, S.; Kolemen, S.; Sedgwick, A. C.; Gunnlaugsson, T.; James, T. D.; Yoon, J.; Akkaya, E. U. Molecular Logic Gates: The Past, Present and Future. *Chem. Soc. Rev.* **2018**, *47*, 2228–2248.
2. Sato, O.; Iyoda, T.; Fujishima, A.; Hashimoto, K. Photo-induced Magnetization of a Cobalt-Iron Cyanide. *Science* **1996**, *272*, 704–705.
3. Lu, Y.-L.; Lan, W.-L.; Shi, W.; Jin, Q.-H.; Cheng, P. Photo-Induced Variation of Magnetism in Coordination Polymers with Ligand-Based Electron Transfer. *Dalton Trans.* **2021**, *50*, 13124–13137.
4. Liu, K.; Zhang, X.; Meng, X.; Shi, W.; Cheng, P.; Powell, A. K. Constraining the Coordination Geometries of Lanthanide Centers and Magnetic Building Blocks in Frameworks: A New Strategy for Molecular Nanomagnets. *Chem. Soc. Rev.* **2016**, *45*, 2423–2439.
5. Zhao, L.; Meng, Y.-S.; Liu, Q.; Sato, O.; Shi, Q.; Oshio, H.; Liu, T. Switching the Magnetic Hysteresis of an [Fe^{II}–NC–W^{V}]-Based Coordination Polymer by Photoinduced Reversible Spin Crossover. *Nat. Chem.* **2021**, *13*, 698–704.
6. Meng, X.; Shi, W.; Cheng, P. Magnetism in One-Dimensional Metal–Nitronyl Nitroxide Radical System. *Coord. Chem. Rev.* **2019**, *378*, 134–150.
7. Gou, X.; Liu, N.; Wu, Y.; Lan, W.-L.; Wang, M.; Shi, W.; Cheng, P. Modulation of Magnetization Dynamics of an

Citation: *CCS Chem.* **2025**, Just Published. DOI: 10.31635/ccschem.024.202404999
Link to VoR: https://doi.org/10.31635/ccschem.024.202404999

Er(III) Coordination Polymer by the Conversion of a Ligand to a Radical Using UV Light. *Dalton Trans.* **2023**, *52*, 10372–10377.
8. Thorarinsdottir, A. E.; Harris, T. D. Metal-Organic Framework Magnets. *Chem. Rev.* **2020**, *120*, 8716–8789.
9. Zhang, X.; Vieru, V.; Feng, X.; Liu, J.-L.; Zhang, Z.; Na, B.; Shi, W.; Wang, B.-W.; Powell, A. K.; Chibotaru, L. F.; Gao, S.; Cheng, P.; Long, J. R. Influence of Guest Exchange on the Magnetization Dynamics of Dilanthanide Single-Molecule-Magnet Nodes Within a Metal-Organic Framework. *Angew. Chem. Int. Ed.* **2015**, *54*, 9861–9865.
10. Liu, J.-L.; Chen, Y.-C.; Tong, M.-L. Symmetry Strategies for High Performance Lanthanide-Based Single-Molecule Magnets. *Chem. Soc. Rev.* **2018**, *47*, 2431–2453.
11. Kragskow, J. G. C.; Mattioni, A.; Staab, J. K.; Reta, D.; Skelton, J. M.; Chilton, N. F. Spin–Phonon Coupling and Magnetic Relaxation in Single-Molecule Magnets. *Chem. Soc. Rev.* **2023**, *52*, 4567–4585.
12. Han, S.-D.; Hu, J.-X.; Li, J.-H.; Wang, G.-M. Anchoring Polydentate N/O-Ligands in Metal Phosphite/Phosphate/Phosphonate (MPO) for Functional Hybrid Materials. *Coord. Chem. Rev.* **2023**, *475*, 214892.
13. Wang, L.-F.; Qiu, J.-Z.; Liu, J.-L.; Chen, Y.-C.; Jia, J.-H.; Jover, J.; Ruiz, E.; Tong, M.-L. Modulation of Single-Molecule Magnet Behaviour via Photochemical [2+2] Cycloaddition. *Chem. Commun.* **2015**, *51*, 15358–15361.
14. Hojorat, M.; Sabea, H. A.; Norel, L.; Bernot, K.; Roisnel, T.; Gendron, F.; Guennic, B. L.; Trzop, E.; Collet, E.; Long, J. R.; Rigaut, S. Hysteresis Photomodulation via Single-Crystal-to-Single-Crystal Isomerization of a Photochromic Chain of Dysprosium Single-Molecule Magnets. *J. Am. Chem. Soc.* **2020**, *142*, 931–936.
15. Huang, X.-D.; Wen, G. H.; Bao, S.-S.; Jia, J. G.; Zheng, L.-M. Thermo- and Light-Triggered Reversible Interconversion of Dysprosium-Anthracene Complexes and Their Responsive Optical, Magnetic and Dielectric Properties. *Chem. Sci.* **2021**, *12*, 929–937.
16. Khariushin, I. V.; Ovsyannikov, A. S.; Islamov, D. R.; Samigullina, A. I.; Solovieva, S. E.; Zakrzewski, J. J.; Chorazy, S.; Ferlay S. Tuning Crystal Packing and Magnetic Properties in a Series of [Dy_{12}] Metallocubanes Based on Azobenzene Derivatives of Salicylic Acid. *Inorg. Chem.* **2023**, *62*, 10548–10558.
17. Zhang, Q.; Han, S.-D.; Li, Q.; Hu, J.-X.; Wang, G.-M. Electron Transfer Photochromism of Ln-Based (Ln = Dy, Tb) Coordinated Polymers for Reversibly Switching Off/On Single-Molecule Magnetic Behavior. *Sci. China Mater.* **2022**, *65*, 788–794.
18. Ma, Y.-J.; Hu, J.-X.; Han, S.-D.; Pan, J.; Li, J.-H.; Wang G.-M. Manipulating On/Off Single-Molecule Magnet Behavior in a Dy(III)-Based Photochromic Complex. *J. Am. Chem. Soc.* **2020**, *142*, 2682–2689.
19. Cai, L.-Z.; Guo, P.-Y.; Wang, M.-S.; Guo, G.-C. Photoinduced Magnetic Phase Transition and Remarkable Enhancement of Magnetization for a Photochromic Single-Molecule Magnet. *J. Mater. Chem. C* **2021**, *9*, 2231–2235.
20. Jiang, S.-D.; Qin, S.-X. Prediction of the Quantized Axis of Rare-Earth Ions: The Electrostatic Model with Displaced Point Charges. *Inorg. Chem. Front.* **2015**, *2*, 613–619.
21. Rinehart, J. D.; Long, J. R. Exploiting Single-Ion Anisotropy in the Design of f-Element Single-Molecule Magnets. *Chem. Sci.* **2011**, *2*, 2078–2085.
22. Li, Q.-W.; Liu, J.-L.; Jia, J.-H.; Chen, Y.-C.; Liu, J.; Wang, L.-F.; Tong, M.-L. "Half-Sandwich" Yb^{III} Single-Ion Magnets with Metallacrowns. *Chem. Commun.* **2015**, *51*, 10291–10294.
23. Errulat, D.; Harriman, K. L. M.; Galico, D. A.; Kitos, A. A.; Mansikkamaki, A.; Murugesu, M. A Trivalent 4f Complex with Two Bis-Silylamide Ligands Displaying Slow Magnetic Relaxation. *Nat. Chem.* **2023**, *15*, 1100–1107.
24. Mondal, A.; Konar, S. A Remarkable Energy Barrier for Spin Reversal in a Field Induced Dinuclear Ytterbium Single Molecule Magnet. *Dalton Trans.* **2021**, *50*, 13666–13670.
25. Mariichak, O.Y.; Kaabel, S.; Karpichev, Y. A.; Rozantsev, G. M.; Radio, S. V.; Pichon, C.; Bolvin, H.; Sutter, J.-P. Crystal Structure and Magnetic Properties of Peacock-Weakley Type Polyoxometalates $Na_9[Ln(W_5O_{18})_2]$ (Ln = Tm, Yb): Rare Example of Tm(III) SMM. *Magnetochemistry* **2020**, *6*, 53.
26. Chorazy, S.; Rams, M.; Wang, J.; Sieklucka, B.; Ohkoshi, S. I. Octahedral Yb(III) Complexes Embedded in $[Co^{III}(CN)_6]$-Bridged Coordination Chains: Combining Sensitized Near-Infrared Fluorescence with Slow Magnetic Relaxation. *Dalton Trans.* **2017**, *46*, 13668–13672.
27. Fan, X.; Freslon, S.; Daiguebonne, C.; Le Pollès, L.; Calvez, G.; Bernot, K.; Yi, X.; Huang, G.; Guillou, O. A Family of Lanthanide-Based Coordination Polymers with Boronic Acid as Ligand. *Inorg. Chem.* **2015**, *54*, 5534–5546.
28. Echenique-Errandonea, E.; Mendes, R. F.; Figueira, F.; Choquesillo-Lazarte, D.; Beobide, G.; Cepeda, J.; Ananias, D.; Rodriguez-Dieguez, A.; Almeida Paz, F. A.; Seco, J. M. Multifunctional Lanthanide-Based Metal-Organic Frameworks Derived from 3-Amino-4-hydroxybenzoate: Single-Molecule Magnet Behavior, Luminescent Properties for Thermometry, and CO_2 Adsorptive Capacity. *Inorg. Chem.* **2022**, *61*, 12977–12990.
29. Li, Q.; Zhang, Q.; Wei, W.-J.; Wang, A-N.; Hu, J.-X.; Wang, G.-M. Light Actuated Stable Radicals of the 9-Anthracene Carboxylic Acid for Designing New Photochromic Complexes. *Chem. Commun.* **2021**, *57*, 4295–4298.
30. Lan, J.-F.; Li, J.; Zhu, J.-L.; Yan, G.-P.; Ke, H.; Liao, J.-Z. Radical-Doped Crystalline Lanthanide-Based Photochromic Complexes: Self-Assembly Driven by Multiple Interactions and Photoswitchable Luminescence. *Inorg. Chem.* **2021**, *60*, 14286–14293.
31. Li, G.-P.; Zhu, H.; Hao, P.; Shen, J.; Fu, Y. The Modulation Effect of Carboxylic Acid Ligands on the Electron Transfer Photochromism of NDI-Derived Coordination Polymers. *Dalton Trans.* **2021**, *50*, 15153–15161.
32. Jin, P.-B.; Luo, Q.-C.; Gransbury, G. K.; Vitorica-Yrezabal, I. J.; Hajdu, T.; Strashnov, I.; McInnes, E. J. L.; Winpenny, R. E. P.; Chilton, N. F.; Mills, D. P.; Zheng, Y.-Z. Thermally Stable Terbium(II) and Dysprosium(II) Bis-amidinate Complexes. *J. Am. Chem. Soc.* **2023**, *145*, 27993–28009.
33. Wang, C.; Sun, R.; Chen, Y.; Wang, B.-W.; Wang, Z.-M.; Gao S. Assembling High-Temperature Single-Molecule Magnets with Low-Coordinate Bis(amido) Dysprosium Unit $[DyN_2]^+$ via Cl–K–Cl Linkage. *CCS Chem.* **2020**, *2*, 362–368.

Citation: *CCS Chem.* **2025**, Just Published. DOI: 10.31635/ccschem.024.202404999
Link to VoR: https://doi.org/10.31635/ccschem.024.202404999

34. Zhang, P.; Zhang, L.; Lin, S.-Y.; Xue, S.; Tang J. Modulating Magnetic Dynamics of Dy_2 System Through the Coordination Geometry and Magnetic Interaction. *Inorg. Chem.* **2013**, *52*, 4587–4592.
35. Zhang, P.; Luo, Q.-C.; Zhu, Z.; He, W.; Song, N.; Lv, J.; Wang, X.; Zhai, Q.-G.; Zheng, Y.-Z.; Tang, J. Radical-Bridged Heterometallic Single-Molecule Magnets Incorporating Four Lanthanoceniums. *Angew. Chem. Int. Ed.* **2023**, *62*, e202218540.
36. Zhang, Q.; Wei, W.-J.; Li, Q.; Pan, J.; Han, S.-D; Hu, J.-X.; Wang, G.-M. Light Enhanced Proton Conductivity in a Terbium Phosphonate Photochromic Chain Complex. *Sci. China Chem.* **2021**, *64*, 1170–1176.
37. Gao, Z.-N.; Feng, D.-X.; Wang, Y.; Li, F.-H.; Sun, H.-Y.; Hu, J.-X.; Wang G.-M. Large Room Temperature Magnetization Enhancement in a Copper-Based Photoactive Metal-Organic Framework. *Inorg. Chem.* **2022**, *61*, 15812–15816.
38. Wang, Y.-X.; Ma, Y.-N.; Chai, Y.-S.; Shi, W.; Sun, Y.; Cheng, P. Observation of Magnetodielectric Effect in a Dysprosium-Based Single-Molecule Magnet. *J. Am. Chem. Soc.* **2018**, *140*, 7795–7798.
39. Lyu, D. P.; Zheng, J.-Y.; Li, Q.-W.; Liu J.-L.; Chen, Y.-C.; Jia, J.-H.; Tong, M.-L. Construction of Lanthanide Single-Molecule Magnets with the "Magnetic Motif" $[Dy(MQ)_4]^-$. *Inorg. Chem. Front.* **2017**, *4*, 1776–1782.
40. Dhbaibi, K.; Grasser, M.; Douib, H.; Dorcet, V.; Cador, O.; Vanthuyne, N.; Riobe, F.; Maury, O.; Guy, S.; Bensalah-Ledoux, A.; Baguenard, B.; Rikken, G. L. J. A.; Train,C.; Le Guennic, B.; Atzori, M.; Pointillart, F.; Crassous, J. Multifunctional Helicene-Based Ytterbium Coordination Polymer Displaying Circularly Polarized Luminescence, Slow Magnetic Relaxation and Room Temperature Magneto-Chiral Dichroism. *Angew. Chem. Int. Ed.* **2023**, *62*, e202215558.
41. Liu, J.-L.; Yuan, K.; Leng, J.-D.; Ungur, L.; Wernsdorfer, W.; Guo, F.-S.; Chibotaru, L. F.; Tong, M.-L. A Six-Coordinate Ytterbium Complex Exhibiting Easy-Plane Anisotropy and Field-Induced Single-Ion Magnet Behavior. *Inorg. Chem.* **2012**, *51*, 8538–8544.
42. Borah, A.; Dey, S.; Gupta, S. K.; Walawalkar, M. G.; Rajaraman, G.; Murugavel, R. Enhancing the Barrier Height for Yb(III) Single-Ion Magnets by Modulating Axial Ligand Fields. *Chem Commun.* **2020**, *56*, 11879–11882.
43. McClain, K. R.; Gould, C. A.; Chakarawet, K.; Teat, S. J.; Groshens, T. J.; Long, J. R.; Harvey, B. G. High-Temperature Magnetic Blocking and Magneto-Structural Correlations in a Series of Dysprosium(III) Metallocenium Single-Molecule Magnets. *Chem. Sci.* **2018**, *9*, 8492–8503.
44. Wang, M.; Guo, Y.; Han, Z.; Cheng, X.; Zhang, Y.-Q.; Shi, W.; Cheng, P. Impact of Ligand Substituents on the Magnetization Dynamics of Mononuclear Dy^{III} Single-Molecule Magnets. *Inorg. Chem.* **2022**, *61*, 9785–9791.
45. Gatteschi, D.; Sessoli, R.; Villain, J. *Molecular Nanomagnets*; Oxford University Press: New York, **2006**.
46. Shrivastava, K. N. Theory of Spin-Lattice Relaxation. *Phys. Stat. Sol.* **1983**, *117*, 437–458.
47. Chakarawet, K.; Bunting, P. C.; Long, J. R. Large Anisotropy Barrier in a Tetranuclear Single-Molecule Magnet Featuring Low-Coordinate Cobalt Centers. *J. Am. Chem. Soc.* **2018**, *140*, 2058–2061.
48. Mondal, A.; Konar, S. Strong Equatorial Crystal Field Enhances the Axial Anisotropy and Energy Barrier for Spin Reversal Process in Yb_2 Single Molecule Magnets. *Chem.–Eur. J.* **2021**, *27*, 3449–3456.
49. Chen, W.-B.; Zhong, L.; Zhong, Y.-J.; Zhang, Y.-Q.; Gao, S.; Dong, W. Understanding the Near-Infrared Fluorescence and Field-Induced Single-Molecule-Magnetic Properties of Dinuclear and One-Dimensional-Chain Ytterbium Complexes Based on 2-Hydroxy-3-methoxybenzoic acid. *Inorg. Chem. Front.* **2020**, *7*, 3136–3145.
50. Gonzalez, J. F.; Douib, H.; Le Guennic, B.; Pointillart, F.; Cador, O. Ytterbium-Centered Isotopic Enrichment Leading to a Zero-Field Single-Molecule Magnet. *Inorg. Chem.* **2021**, *60*, 540–544.
51. Habib, F. P.; Lin, H.; Long, J.; Korobkov, I.; Wernsdorfer, W.; Murugesu M. The Use of Magnetic Dilution to Elucidate the Slow Magnetic Relaxation Effects of a Dy_2 Single-Molecule Magnet. *J. Am. Chem. Soc.* **2011**, *133*, 8830–8833.
52. Ungur, L.; Chibotaru, L. F. *Computational Modelling of the Magnetic Properties of Lanthanide Compounds*; Wiley-VCH Verlag GmbH & Co. KGaA: Germany, **2015**.
53. Neese, F.; Wennmohs, F.; Becker, U.; Riplinger, C. The ORCA Quantum Chemistry Program Package. *J. Chem. Phys.* **2020**, *152*, 224108.
54. Neese, F. Software Update: The ORCA Program System-Version 5.0. *WIREs Comput. Mol. Sci.* **2022**, *12*, e1606.

Citation: *CCS Chem.* **2025**, Just Published. DOI: 10.31635/ccschem.024.202404999
Link to VoR: https://doi.org/10.31635/ccschem.024.202404999